A Quasi-Steady Model for the Lift on a Hovering Flexible Wing

Chang-kwon Kang[1*] and Wei Shyy[2†]

*Department of Mechanical and Aerospace Engineering, University of Alabama in Huntsville
Huntsville, AL, 35899*

†*Department of Mechanical and Aerospace Engineering, Hong Kong University of Science and Technology
Clear Water Bay, Hong Kong*

In the analysis of flexible flapping wing, the aerodynamic outcome resulting from the combined structural dynamics and the unsteady fluid physics of the wing depends on the instantaneous angle of attack (AoA) and wing shape, which are *a priori* unknown. To offer a simplified and effective framework to address such challenges, we propose an analytic model to predict the unsteady lift on a hovering flexible wing. We model the fluid dynamic force with the Morison equation to estimate the instantaneous AoA, resulting from passive pitch. The corresponding unsteady lift is obtained using a quasi-steady model. Besides the imposed plunge amplitude, the model inputs are the scaling parameters accounting for the wing thickness, density, and stiffness. The structural damping coefficient is empirically determined. The predicted time histories of the passive pitch and lift can satisfactorily mimic the high fidelity aeroelastic solutions. Such analytic models of instantaneous wing deformation and lift generation improve our understanding of flexible flapping wing aerodynamics and can be used as fast yet reliable tools for design analysis.

Nomenclature

c	= chord	[m]
c_d	= structural damping coefficient	[1]
C_L	= coefficient of lift	[1]
C_v	= aerodynamic damping coefficient	[1]
E	= Young's modulus	[Pa]
f	= motion frequency	[1/s]
f_1	= first natural frequency of the wing	[1/s]
F	= fluid force acting on the wing per unit length	[N/m]
h	= plunge motion of the wing	[m]
h_a	= plunge amplitude	[m]
h_s	= thickness of the wing	[m]
k	= reduced frequency, $\pi f c/U$	[1]
K_C	= Keulegan-Carpenter number, π/k	[1]
p	= pressure	[Pa]
Re	= Reynolds number, Uc/ν	[1]
St	= Strouhal number, fh_a/U	[1]
t	= time	[s]
T	= period of the motion stroke, $1/f$	[s]
U	= reference velocity: $2\pi fh_a$ for hover	[m/s]

[1]Assistant Professor, Department of Mechanical and Aerospace Engineering, University of Alabama in Huntsville, AIAA Member.

[2]Provost & Chair Professor, Department of Mechanical and Aerospace Engineering, Hong Kong University of Science and Technology, AIAA Fellow.

u	= velocity	[m/s]
v	= wing displacement: $v=w+h$	[m]
w	= wing deformation relative to the imposed motion h	[m]
α	= passive pitch angle	[°]
α_a	= angular amplitude	[°]
α_m	= midstroke passive pitch angle	[°]
α_e	= end-of-the-stroke passive pitch angle	[°]
β	= coefficient for the aerodynamic damping term	[1]
γ	= non-dimensional tip deformation parameter: $2(1+\pi/4\rho^* h_s^*)/\{k\,(f_1^2/f^2-1)\}$	[1]
δ	= coefficient for the acceleration related term	[1]
ζ	= coefficient for the structural damping term	[1]
φ	= phase lag between rotational and translational motion	[°]
ν	= kinematic viscosity of fluid	[m²/s]
Π_0	= effective inertia: $\rho^* h_s^* (k/\pi)^2$	[1]
Π_1	= effective stiffness: $E h_s^{*3}/(12\rho_f U^2)$	[1]
ρ_f	= density of fluid	[kg/m³]
ρ_s	= density of structure	[kg/m³]
$(\cdot)^*$	= variables normalized either by c (length), $1/f$ (time), or ρ_f (density)	
$(\overline{})$	= time-averaged variables	

I. Introduction

Biological flyers offer many the desirable flight characteristics that can be applied to the design of Micro-Air Vehicles[1] (MAVs). They can rapidly accelerate and decelerate in confined spaces as well as exhibit spectacular maneuvers to avoid obstacles and to conduct flight missions. For example, a hummingbird frequently utilizes wing-tail combination with rapid shape changes to respond to wind gusts. The wings of biological flyers, especially those of small birds, insects, and bats are flexible and can substantially deform during flight. As a result, the aerodynamics, structural dynamics, and flight dynamics are closely linked to each other. Wing motion affects the fluid force on the wing, which in turn leads to changes in the wing shapes and motions. These highly coupled nonlinearities make the successful design of MAVs challenging.

For the design and development of conventional passenger airplanes, abstracted model tests have greatly enhanced the understanding of the fluid physics around the aircraft wings, engines, or even the whole airplane[2]. Such a model testing is necessary, especially when the behavior of a specific airplane is so complex that a simplified theoretical analysis becomes doubtful[2]. Although full-scale wind tunnels exist, most experiments are performed on a scale models by satisfying the requirements of the geometric similarity and the dynamic similarity. Furthermore, when the governing equations are known, certain conditions of dynamic similarity may be omitted without loss of exactness[2] and the rather general outcome from the dimensional analysis can be reduced to a simpler scaling relationship as a property of the special problem under consideration. These scaling parameters can identify the main physical principle in a complex model and greatly simplify the model design and testing.

One of the main challenges of the study of flexible flapping wing aerodynamics is that the wing shape and motion result from the dynamic balance between the wing inertial force, elastic restoring force, and fluid dynamic force and such information is not known *a priori* and complex. In our previous investigations, we have established that there exists scaling relationships between time-averaged aerodynamic performance and the relative shape deformation amplitude, based on the so-called γ-parameter[3]. These scaling relationships are useful for the preliminary design phase of MAVs as they provide an estimate for the expected propulsive force or efficiency as a function of the structural parameters and wing kinematics. For insects, with a notable exception of butterfly, since the flapping time is much faster than that of the vehicle, the instantaneous information from flapping may not be as critical[1]. Nevertheless, to model the flight dynamics for the analysis of stability and control of a flight vehicle, better instantaneous aerodynamic force models are needed for improved time-averaged estimate, and both require a formulation for the wing deformation and motion as a function of time.

Recently, we proposed a model to analyze and estimate the instantaneous wing deformation[4]. We considered a passive pitch, active plunge motion of a two-dimensional wing in hover at $Re=Uc/\nu=100$, based on the midstroke

American Institute of Aeronautics and Astronautics

velocity U, wing chord length c, and kinematic viscosity of fluid ν. A sinusoidal plunge motion h with amplitude h_a and frequency f is imposed on the leading-edge (LE) of the wing as

$$h(t) = h_a \cos(2\pi f t) \tag{1}$$

as a function of time t, see also Fig. 1. In the absence of freestream for hovering flight, we set the maximum translational velocity U of the flat plate at the LE as the reference velocity, such that $U=2\pi f h_a$[5–7]. Note that reduced frequency in hover becomes a geometric quantity: $k=\pi f c/U=c/(2h_a)$. The Strouhal number, another important parameter in flapping wing aerodynamics, becomes a constant for hovering motions: $St = f h_a/U = 1/(2\pi)$. We modeled the wing as a linear elastic flat plate and the fluid forces using the Morison equation[8], modeling for the added mass and aerodynamic damping forces at low Reynolds numbers. The Keulegan-Carpenter number, often used in discussion of the Morison equation[8], is inversely proportional to the reduced frequency $K_C = \pi/k$. The added mass force is caused by the acceleration of the wing and is linearly proportional to the wing acceleration in the linearized aerodynamics theories. The aerodynamic damping forces are associated with the vortices in the flow field and depend on the square of the motion velocity. Obtained formulation compared favorably, albeit with a correction for the midstroke angle, against numerical data, which are computed using a fully-coupled Navier-Stokes aeroelastic solver[7].
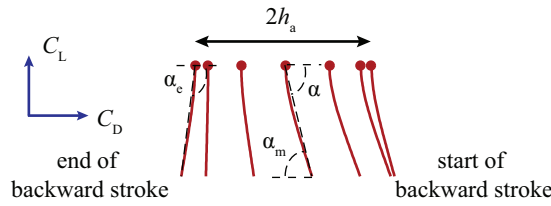

Figure 1. Schematic of the wing motion with amplitude h_a. Wing deformations lead to a passive pitch angle α. The angles at the mid and end-of-the-strokes are α_m and α_e, respectively. The directions of the lift and drag are normal and parallel to the imposed plunge motion, respectively. Leading-edge of the wing is represented with a red dot. From Kang and Shyy[7].

The objective of this study is to develop a simplified model to predict the instantaneous aerodynamic lift generation of a hovering flexible wing. The use of simplified models is in general limited by the lack of information of key aerodynamic coefficients, which we address with the insight gained from our previous high fidelity simulations and experimental observations from the literature. For the aerodynamic damping coefficient[8] in the Morison equation we use an empirical formula as a function of the Reynolds number and the reduced frequency k. We then use the quasi-steady model by Dickinson and co-workers[7,9] to calculate the resulting lift on a wing that translates with the imposed plunge motion and rotates with the estimated pitch angle. The fundamental principle of a quasi-steady model is that the fluid dynamic forces depend on the instantaneous wing velocities and accelerations. Therefore, a quasi-steady model neglects the influence from the history effects. For example, the nonlinear wing-wake interaction can play a substantial role for hovering motions, which is not included in this quasi-steady model. We assess the performance of the proposed model by comparing the resulting lift against numerical solutions from a fully-coupled aeroelastic solver[7].

II. Methodology

A. Governing Equations for the Fluid-Structure Interaction System

We consider a non-dimensional flow field with unit density initiated by a hovering two-dimensional flat plate with unit chord and flat edges[7]. The flow field is governed by the unsteady Navier-Stokes equations with constant density ρ_f and viscosity

$$\boldsymbol{\nabla}^* \cdot \boldsymbol{u}^* = 0$$
$$\frac{\partial \boldsymbol{u}^*}{\partial t^*} + (\boldsymbol{u}^* \cdot \boldsymbol{\nabla}^*)\boldsymbol{u}^* = -\boldsymbol{\nabla}^* p^* + \frac{1}{Re}\Delta^* \boldsymbol{u}^* \tag{2}$$

3
American Institute of Aeronautics and Astronautics

for the velocity $\boldsymbol{u}$, pressure p, and time t. The superscript (*) indicates non-dimensional variables. The dimensional variables are non-dimensionalized with U, c, and the period of a motion stroke $T=1/f$, respectively.

The wing is an elastic flat plate of uniform thickness h_s, density ρ_s, and Young's modulus E. As the flat plate follows the imposed horizontal motion, Eq. (1), at the LE, the resulting fluid dynamic force dynamically balances with the wing inertia and the elastic bending forces, modeled locally as a linear Euler-Bernoulli beam as

$$\Pi_0 \frac{\partial^2 v^*}{\partial t^{*2}} + c_{\text{d}} \frac{\partial v^*}{\partial t^*} + \Pi_1 \Delta^{*2} v^* = F^*, \tag{3}$$

where v is the displacement due to bending motion, $\Pi_0 = \rho^* h_s^* (k/\pi)^2$ is the effective inertia, the inertia of the wing normalized by the fluid dynamic variables[3], $\rho^* = \rho_s/\rho_f$ is the density ratio between the wing density and the fluid density, c_{d} is the non-dimensional structural damping coefficient, $\Pi_1 = E h_s^{*3}/(12\rho_f U^2)$ is the effective stiffness, the wing stiffness normalized by the fluid dynamic variables[3], and F is the distributed transverse fluid force per unit length on the wing, such that $F^* = F/(\rho_f U^2)$. The resulting wing camber deformations $w = v - h$ can also be regarded as a pitch rotation $\alpha(t^*)$, the angle between the trailing-edge (TE) and LE, see also Fig. 1.

The time-averaged values are indicated with an over-bar, which are defined as

$$\bar{C}_{\text{L}} = f \int_{m/f}^{(m+1)/f} C_{\text{L}} \, dt, \tag{4}$$

for example, for C_{L}. The resulting forces in the numerical computations were not periodic[7] in time and to have a representative value for the time averaged force and to avoid initial transient effects, we choose for $m = 3$. For a more comprehensive treatment of the dimensional analysis and non-dimensionalization we refer to our previous work[3].

B. Navier-Stokes Equation Solver

The governing equations for the fluid given by Eq. (2) were solved using an in-house three-dimensional, unstructured, pressure-based finite volume solver[7,10,11], written in a rule-based framework[12]. It employs implicit first or second order time stepping and treats the convection terms using the second order upwind-type scheme and the pressure and viscous terms using second order schemes. The system of equations resulting from the linearized momentum equations are handled with the symmetric Gauss-Seidel solver. The pressure correction equation is solved with either the GMRES linear solver with the Jacobi preconditioner provided by PETSc[13,14], or the BoomerAMG[15] linear solver provided by hypre. The LOCI-framework is by design rule-based highly parallelizable framework for finite volume methods[12]. The geometric conservation law[16], a necessary consideration in domains with moving boundaries, is satisfied[17]. We use the radial basis function interpolation method to deform the computational mesh at each time step[18]. The boundary conditions for the fluid flow were the incompressible inlet with zero velocity at the outer boundary of the computational domain and no-slip on the flat plate surface. More details including the spatial and temporal sensitivity tests can be found in Kang and Shyy[7].

C. Quasi-steady Model

The quasi-steady model[7,9] used in this study has three components as

$$F = F_{\text{translational}} + F_{\text{rotational}} + F_{\text{added mass}} \tag{5}$$

where the translational force component, which estimates the delayed stall, is computed as

$$F_{\text{translational}} = \frac{1}{2} \rho_f \dot{h}^2 c C_{\text{L,q}}, \tag{6}$$

where $C_{\text{L,q}}$ is the coefficient of lift [19] is

$$C_{L,q} = 0.025 + 1.58 \sin(2.13\alpha - 7.2). \tag{7}$$

Equation (7) is obtained from empirically fitted equations from a 180° sweep with fixed angles of attack using a dynamically scaled fruit-fly wing in mineral oil.

The rotational force term, which is only used for actively rotated rigid wings[7] and represents the coupling term between the translational velocity and the angular velocity, is

$$F_{\text{rotational}} = -C_r \dot{\alpha} c^2 \rho_f \dot{h}, \tag{8}$$

where C_r is an empirical coefficient that depends on the angular velocity. Large pressure differentials exist on actively rotating rigid wings near the trailing edge contribute to the total lift at the ends-of-the-strokes. However, these lift-enhancing rotational effects are relaxed by the compliant nature for a flexible wing[7]. Instead of generating rotational forces, a flexible wing can streamline its wing shape such that the wing shape and motion are in equilibrium with the fluid forces, similar to the drag-reducing reconfiguration of flexible bodies[7].

Finally, the added mass force consists of two components, i.e.

$$F_{\text{added mass}} = F_{\text{added mass},1} + F_{\text{added mass},2} \tag{9}$$

where the non-circulatory term can be written as

$$F_{\text{added mass},1} = \frac{\rho_f \pi c^2}{4} \left(\ddot{h} - \frac{a_h c}{2} \ddot{\alpha} \right) \tag{10}$$

where $a_h = -1$ when the pivot point is located at LE [19]. The first term $F_{\text{added mass},1}$ is linearly proporitonal to the translational and rotational accelerations. The circulatory term is

$$F_{\text{added mass},2} = \frac{\rho_f \pi c^2}{4} \dot{h}\dot{\alpha}, \tag{11}$$

proportional to the coupled translation and rotational velocity terms. The second term $F_{\text{added mass},2}$ describes a damping in pitch which in fact comes from the circulatory part[20].

The nonlinear wing-wake interaction can play a substantial role for hovering motions, which is not included in this quasi-steady model. The complex wake, induced in the previous motion strokes, interacts with the wing during its return stroke. Under favorable conditions, added momentum causes the lift to increase during the first portion of the stroke, which is called a wake-capture[19]. The induced downward wake can also lead to a reduced effective angle of attack, and, hence, to a lower lift. Intriguingly, a flexible wing can streamline its wing shape with the surrounding fluid and mitigate the lift-degrading wing-wake interaction[7]. As a result, the lack of the model for the wing-wake interaction has a less severe effect on the estimation of the lift on a flexible wing than for a rigid wing.

III. Results and Discussion

A. Case Setup

We compare the passive pitch angle and the unsteady lift on a flexible flapping wing with the results obtained from Navier-Stokes equation computations fully coupled to a structural dynamics solver[7].

For the numerical computations, the Reynolds number was $Re=100$, relevant to a fruit fly. The density ratio is $\rho^*=7.8$ and the thickness ratio is $h_s^*=0.02$. The reduced frequency range of $0.25<k<3.04$ is motivated from the selection of h_a of biological relevance[7]. The frequency ratio is in the range of $0.08 \le f/f_1 < 0.40$, which results in advanced and symmetric rotational modes, also motivated from the previous findings that the natural flyers operate at a frequency ratio less than the first natural frequency[21]. The natural frequency f_1 is measured in the chordwise direction between the LE and TE. More details on the case setup can be found in Kang and Shyy[7].

American Institute of Aeronautics and Astronautics

B. Scaling of the Force on the Wing

The coupled fluid dynamics and the structural dynamics of the flow around the wing and the wing shape deformations and displacements simultaneously satisfy Eqs. (2) and (3), the Navier-Stokes equation and the beam equation, respectively. To model the dynamics of the structural response, we analyze the physics based on Eq. (3) with simplifying approximations for the fluid dynamic force F^*. The Navier-Stokes equation is nonlinear in its convection term and a full explicit expression for F^* is not available.

The fluid dynamic force is often decomposed into two terms, the added mass force and the force induced by the vorticity in the flow field[3,22], or the aerodynamic damping force term.

The added mass force is caused by the acceleration of the wing and is linearly proportional to the wing acceleration in the linearized aerodynamics theories. With increasing k, the added mass force gains its relative contribution to the total fluid dynamic force[7]. Based on scaling arguments, we found that, for the deformation of flexible flapping wings, the fluid dynamics force term could be well approximated by the added mass force for various cases at $k>O(1)$ and $Re>O(10^2)$[3]. Moreover, based on Eq. (3) we derived scaling relationships between the aerodynamic performance, such as the time-averaged propulsive force and the propulsive efficiency, and the relative shape deformation parameter γ defined as

$$\gamma = \frac{St\, k \left(1+\frac{4}{\pi}\rho^* h_s^*\right)}{\Pi_0(f_1^2/f^2 - 1)},$$ (12)

where γ can be obtained from *a priori* determined parameters. For the parameters used in the numerical computations, i.e. $\rho^*=7.8$, $h_s^*=0.02$, and k of around 0.6 result in a relation between γ and f/f_1, which is in a comparable range for the typical values for fruit flies with $\rho^*=1100$, $h_s^*=0.6\times10^{-3}$, and $k = 0.212$[7]. This implies that the effects of f/f_1 on γ given by Eq. (12) in this study will be similar to that of a fruit fly.

In our previous work[3], we proposed a scaling relationship, see also Fig. 2 for the revised version of the scaling, between the time-averaged force $\bar{C}_F$ on the flexible flapping wing and γ as

$$\frac{\bar{C}_F}{\Pi_1}\sim\gamma\,,$$ (13)

which is consistent with the scaling relationship that was based on an experiment in air[21,23], where γ becomes equivalent to the elastoinertial number $\mathcal{N}_{ei}$ for air[3]. More recently, similar experiment has been performed in water[24] from which a scaling relationship was found as

$$\frac{F_T c}{E h_s^3}\frac{1}{AR}\sim f^*\,,$$ (14)

for the thrust F_T and the aspect ratio AR. The frequency ratio f^* was empirically determined by locating the maximum wing tip deflection, which includes the effects of added mass. It can be shown that the empirically determined scaling for flapping wings in water, Eq. (14), is also consistent with the scaling that we proposed, Eq. (13), since

$$\frac{\bar{C}_F}{\Pi_1} = \frac{F}{\frac{1}{2}\rho_f U^2 S}\bigg/ \frac{E h_s^3}{12\rho_f U^2 c^3} = \frac{Fc}{E h_s^3}\frac{24}{AR} \sim \frac{Fc}{E h_s^3}\frac{1}{AR}$$ (15)

for the LHS of Eq. (14), where $S=AR\, c^2$ is the area of a rectangular wing. In our study, we considered the added mass as an external fluid dynamic force, which is included in the definition of γ. Alternatively, since added mass is proportional to the acceleration, a modified natural frequency can be established that includes the effects of added mass, i.e. the empirical frequency ratio f^*[24].

The scaling given by Eq. (13) was further revised[7] with a correction factor to account for a wider range of f/f_1 as

$$\bar{C}_L^* = \frac{\bar{C}_L}{\Pi_1\{1 - (f/f_1)^2\}}k\sim\gamma.$$ (16)

These scaling relationships cover a wide variety of wing flexibility and flapping characteristics relevant to insects as well as artificially-devised flexible wings, see Fig. 2a. Moreover, γ can be interpreted as a non-dimensional TE displacement relative to the LE[7]. The chordwise wing deformation of the wing acts as passive pitch with an angle of attack α, which forms the main idea of this study. Figure 2b illustrates the link between the normalized maximum pitch angle during a stroke, α^*_{max}, and the scaling parameter γ. The normalization is given in Eq. (16). A linear fit to the numerically determined data is

$$\alpha^*_{max,pred} = 0.804 \log \gamma - 1.312 \tag{17}$$

with a coefficient of determination of $R^2 = 0.98$. The predicted maximum angle $\alpha_{max,pred}$ for advanced and symmetric rotation cases correlates well with the numerically determined values of α_{max}, as shown in Fig. 2c.
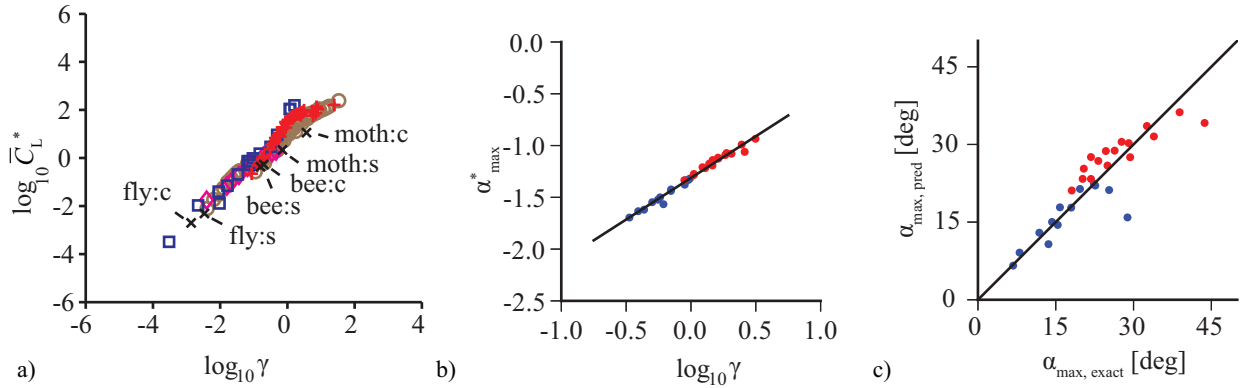

Figure 2. Scaling relationships between the normalized lift $\overline{C}_L{}^*$, normalized maximum pitch angle α_{max}, and γ. Reynolds number is $Re = 100$. (a) Scaling of $\overline{C}_L{}^*$ by γ (+). From Kang and Shyy[7]. The current dataset is plotted together with data from the literature for a chordwise (○), spanwise (◇), isotropic (□) wing, and insects (×), where the lift for the insects are etimated by their weight. (b) Scaling between α^*_{max} and γ. (c) Comparison between the predicted maximum angle $\alpha_{max, pred}$ using the scaling relationship determined in (b) and α_{max} from a high fidelity model[7]. In (b,c), (●): advanced rotation; (●): symmetric rotation.

Although the scaling in terms of the added mass, given in Fig. 2b, can be used to determine the passive pitch amplitude, the aerodynamic damping augments the fluid dynamic force on a flapping wing. Therefore, in order to predict the instantaneous, dynamic response of the wing motion including the wing deformations with a better accuracy, we model the fluid dynamic force F on the moving wing as[4]

$$F = F_a + F_v = \frac{\pi}{4}\rho_f c^2 \frac{d^2 h}{dt^2} + \frac{1}{2}\rho_f \frac{dh}{dt}\left|\frac{dh}{dt}\right| C_v c, \tag{18}$$

which is the Morison equation[8] for the dimensional fluid dynamic force per unit length F. We model the added mass force F_a with the classic solution for the force acting normal to a thin flat plate with chord c moving with $h(t)$. The second term F_v is the aerodynamic damping term which is proportional to the square of the wing velocity. The aerodynamic damping coefficient C_v depends on k, Re, etc. in general[8] and may also be a function of space and time. Here, we use Eq. (19), which is based on a series of drag force measurements[8] on an oscillating rigid flat plate in a water tank for various $K_C = \pi/k$ and Re as

$$C_v = 15 K_C^{-0.5} \exp\left(\frac{1.88}{Re^{0.547}}\right). \tag{19}$$

Equation (19) indicates that C_v is proportional to $k^{0.5}$. Also the magnitude this aerodynamic damping term C_v increases when the relative importance of the viscous effects become more important, with reducing Reynolds number.

C. Instantaneous Passive Pitch Model

The solution of the governing equation for the structural dynamics of the wing given by Eq. (3) with the fluid dynamic force Eq. (18) results in the trailing-edge displacement w_e relative to the leading-edge at the end and mistrokes as[4]

$$w_e = \frac{\delta\left\{-1+\left(\frac{f_1}{f}\right)^2\right\}+\frac{(\delta-1)\zeta^2}{2\pi}}{4\pi^2\left\{-1+\left(\frac{f_1}{f}\right)^2\right\}^2+\zeta^2} - \frac{\beta}{2}\left[\frac{1}{4\pi^2}\left(\frac{f}{f_1}\right)^2 - \frac{\left\{-4+\left(\frac{f_1}{f}\right)^2\right\}}{4\pi^2\left\{-4+\left(\frac{f_1}{f}\right)^2\right\}^2+4\zeta^2}\right] \tag{20}$$

and

$$w_m = \frac{\zeta\left\{\frac{\delta}{2\pi}-1+\left(\frac{f_1}{f}\right)^2\right\}}{4\pi^2\left\{-1+\left(\frac{f_1}{f}\right)^2\right\}^2+\zeta^2} + \frac{\beta}{2}\left[\frac{1}{4\pi^2}\left(\frac{f}{f_1}\right)^2 - \frac{\left\{-4+\left(\frac{f_1}{f}\right)^2\right\}}{4\pi^2\left\{-4+\left(\frac{f_1}{f}\right)^2\right\}^2+4\zeta^2}\right] \tag{21}$$

respectively, where $\delta=2\pi^2 Stk(1+4\rho^* h_s^*/\pi)/\Pi_0$, $\beta=C_v/\Pi_0$, and the non-dimensional damping factor is $\zeta=c/\Pi_0$. The two terms on the RHS of Eqs. (20) and (21) indicate the effects of the added mass and aerodynamic damping forces, respectively. Note that δ is linked to γ as $\gamma=\delta/2\pi^2\{(f_1/f)^2-1\}$. See also Kang and Shyy[4] for more details on the derivation of Eqs. (20) and (21).
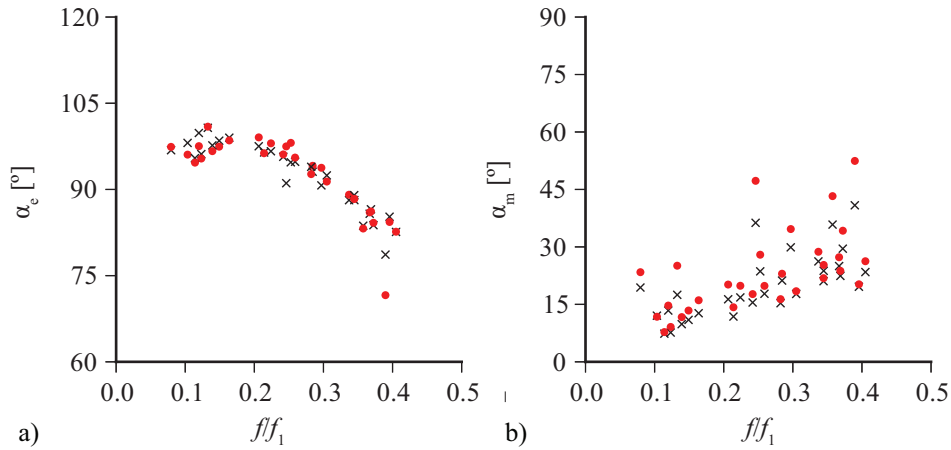

Figure 3. (a) Passive pitch angle α_e at the end-of-the-stroke and (b) α_m at the midstroke as functions of the frequency ratio f/f_1. (●) Current model; (×) High fidelity model of Kang and Shyy[7].

Figure 3 shows the passive pitch angles $\alpha_e=\arctan(w_e)$ and $\alpha_m=\arctan(w_m)$ as functions of f/f_1. The unknown coefficient for the structural damping c_d is empirically determined from the numerical data[7]. Note that in our previous work the reduced frequency is kept as a constant of $k=0.6$, while in this work, we use the corresponding values of k for each case, improving the generality of this model. The correlations between the predicted passive pitch angles and the numerical data is good. For lower frequency ratios $f/f_1<0.19$, α_e increases. In this range, the added mass term has the greatest contribution[4]. As f/f_1 increases further, the aerodynamic damping term starts to play a more dominant role[4]. The rotational mode becomes symmetric at around $f/f_1=0.32$ and decreases further into delayed rotational mode with f/f_1.

Based on the angles α_{max} and α_e, a first-order harmonic approximation for the passive pitch $\alpha_{FH}(t/T)$ can be constructed by solving for the phase lag φ and the angular amplitude α_a, as given by Eq. (22),

$$\alpha_{FH} = 90 - \alpha_a\cos(2\pi t/T + \varphi). \tag{22}$$

It is known that the timing between translation and rotation, indicated by the phase lag φ and the amplitude α_a are critical for lift generation. Specifically, when a rigid wing rotated with an amplitude of $40° < \alpha_a < 50°$ before it reaches the end-of-the-stroke, the highest lift coefficients are obtained[5,19]. This so-called advanced rotation performs better than the symmetric or the delayed rotational modes in which the wing reversal is synchronized or delayed with respect to the translation, respectively. Despite the predicted optimal lift generation at the advanced rotation modes, hovering fruit flies[25], honeybees[6], beetles[26], and hymenopterans exhibit symmetric rotations in general[26]. The gap between the predicted maximum lift generation for advanced rotations and the symmetric rotations exhibited by a wide range of insects can be explained by considering the wing flexibility. Although tethered flying fruit flies actively control the wing rotation timings to initiate yaw turns[27], these natural flyers possess flexible wings that deform significantly during flight that can enhance the aerodynamic performance[28,29]. Hovering flexible flapping wings with an imposed harmonic translational motion at the LE of the wing also generate passive pitch rotations with advanced, symmetric, and delayed rotational modes, where the phase lag strongly correlates to f/f_1[7]. More importantly, these flexible wings produce the highest lift for symmetric rotations, consistent with the reported observations of the aforementioned insects[7].
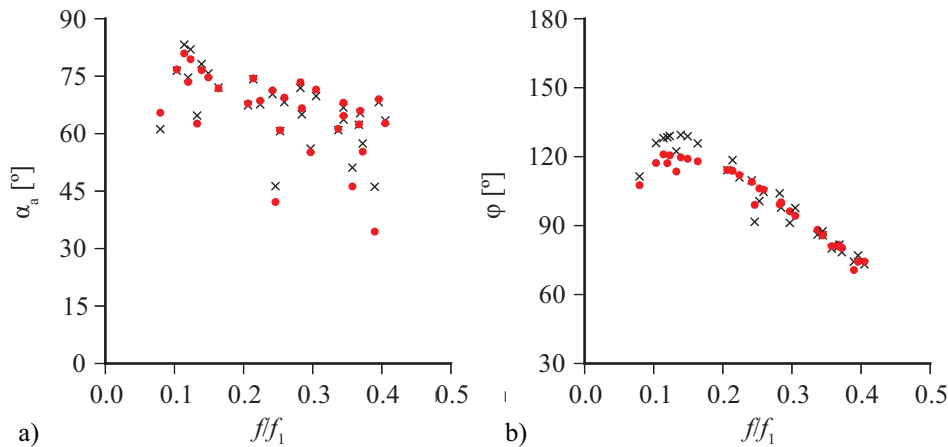

Figure 4. Characterization of the passive pitch based on α_{FH}. (a) Angular amplitude α_a as a function of f/f_1. (b) Phase lag φ as a function of f/f_1. (●) Current model; (×) High fidelity model of Kang and Shyy[7].

The resulting, predicted amplitude α_a is illustrated in Fig. 4a along with the numerically computed values. Despite its complicated behavior in f/f_1, the predicted amplitude shows a good agreement with the numerical results. The phase lag φ underpredicts the lag between the imposed translation and the passive pitch for advanced rotations ($f/f_1 < 0.2$), but the correlation improves for higher f/f_1, see Fig. 4b. Overall, the predicted α_a and φ show strong agreements with the fully coupled numerical solution and is able to capture the critical trend of the relation between the different rotational modes and the frequency ratio. As the model for C_v is determined from measurements on a rigid wing without rotation, the correlation between the predicted angles, given by Eqs. (20) and (21) worsened as the wing deformations increases. Therefore, we only consider $f/f_1 < 0.4$, which corresponds to advanced, symmetric, and delayed rotations with the resulting phase lag $\varphi > 70°$.

With φ and α_a, a first-order harmonic representation of the passive pitch α_{FH} can be determined as a function of time t/T in Eq. (22). The predicted time evolutions of the unsteady passive pitch as a function of time are shown in Fig. 5. We illustrate two representative cases each for advanced (Fig 5a: $k=1.125$, $f/f_1=0.25$; Fig 5b: $k=1.65$, $f/f_1=0.21$) and symmetric (Fig 5c: $k=0.6$, $f/f_1=0.25$; Fig 5d: $k=1.68$, $f/f_1=0.34$) rotational modes. The predicted $\alpha_{FH}(t/T)$ matches well with the time history of passive pitch that is determined from the numerical computations[7]. As predicted by the estimation of the angular amplitude α_a and the phase lag φ in Fig. 4, respectively, there exists certain discrepancies in the detailed shape of the time history of the passive pitch angle due to the involved limitations of the simplified model. For example, we empirically determined the coefficient for the structural damping terms and the aerodynamic damping was obtained for a rigid flat plate without rotation. In principle, these coefficients should be functions of space and time and depend on the Reynolds number and the frequency ratio as well. A detailed study on these coefficients is left as a future study. An improvement over the previous passive pitch model[4] is that we are able to the angular amplitude without any manual correction as shown in Fig. 4a.

For the advanced rotation case in Fig. 5a and the symmetric rotation case Fig. 5c, the estimated phase lag is slightly off. Still, for the most cases, the prediction of the phase lag is accurate, as shown in Figs. 5b,d. The

American Institute of Aeronautics and Astronautics

predicted angular amplitude is reasonable for all cases. Figure 5c shows the case with the largest difference in the amplitude of $\alpha(t/T)$. For this symmetric rotation case, the wing significantly deforms around the midstroke, resulting in a maximum passive pitch angle of 43°. The difference between the maximum angles is evident, also due to the higher harmonic modes in the nonlinear transient structural response[7]. The time history of passive pitch for the symmetric rotation case in Fig. 5d is very well predicted by the current model.
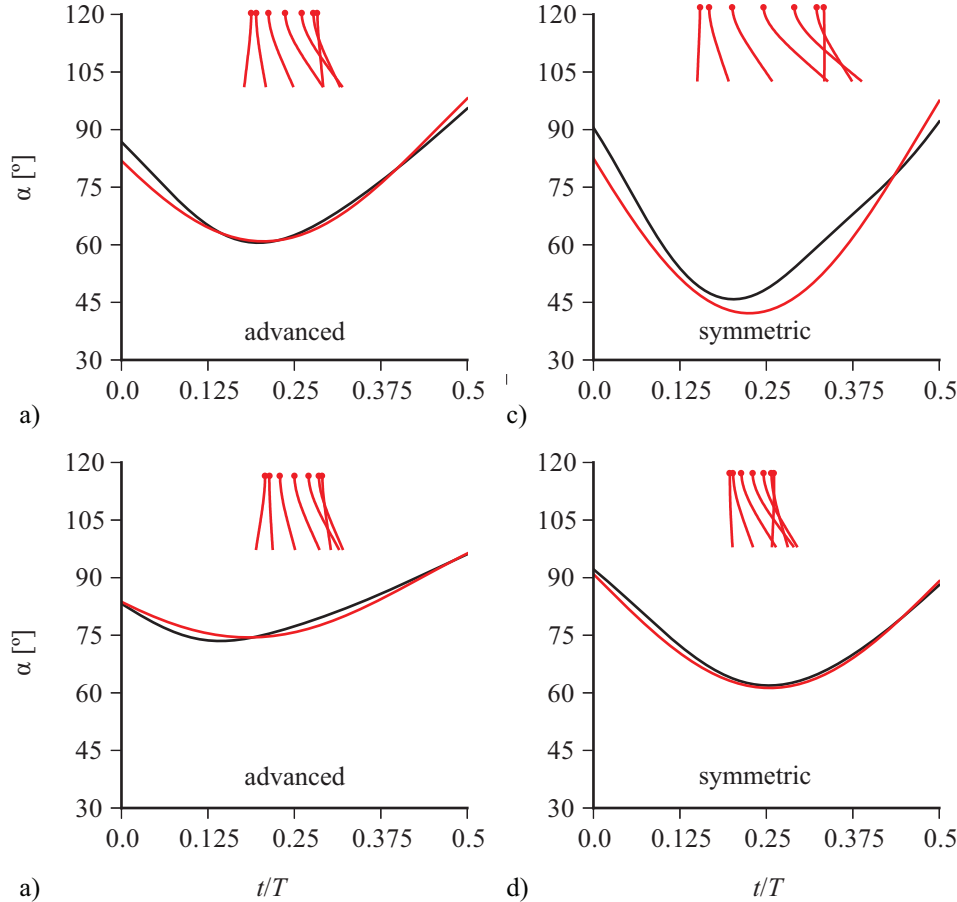

Figure 5. Representative time histories of the passive pitch angle α for (a,b) two advanced rotation and (c,d) symmetric rotation cases. (−) Current quasi-steady model; (−) High fidelity model of Kang and Shyy[7].

D. Instantaneous Lift on a Flexible Flapping Wing

The main objective of this study is to model the unsteady lift generation on a wing as a function of time. The hovering, flexible wing moves with a translational motion given by Eq. (1), imposed on the leading-edge of the wing, and the corresponding wing deformations can be seen as passive wing rotation α_{FH}, given by Eq. (22). Based on these translational and rotational motions, we calculate the lift force $C_L(t/T)$ as a function of the non-dimensional time using the quasi-steady model, described in Section IIC.

The resulting time histories of lift $C_L(t/T)$ are presented in Fig. 6, for the same representative cases as in Fig. 6. Overall, the predicted unsteady lift forced $C_L(t/T)$ agrees well with the time history of lift coefficient, obtained from a fully coupled aeroelastic numerical framework[7]. Since the lift generation on a flexible flapping wing is a consequence of a complex, nonlinear coupling between unsteady aerodynamics and structural dynamics, this simple, analytic model is unable to predict all the details that we obtain from our numerical framework. Indeed, there are differences in both the amplitude and the phase, see e.g. Fig. 6a. Also, the symmetric rotation case that is depicted in Fig. 6d has a relatively well-predicted passive pitch (Fig. 6d), however the predicted lift has an obvious difference in the peak value. Also, the nonlinear wing-wake interaction plays a non-negligible role for hovering motions, which cannot be predicted by the quasi-steady model. The vortices, shed in the previous motion stroke, induce a complex velocity field around the midstroke[30], which in turn interacts with the wing during its return stroke. Under favorable

conditions, added momentum causes the lift to increase during the first portion of the stroke[19], but the induced downward wake can also lead to a reduced effective angle of attack, and, hence, to a lower lift. For flexible wings, on the other hand, the streamlining of the wing shape can lead to lift enhancement by mitigating the lift-degrading wing-wake interaction[7].
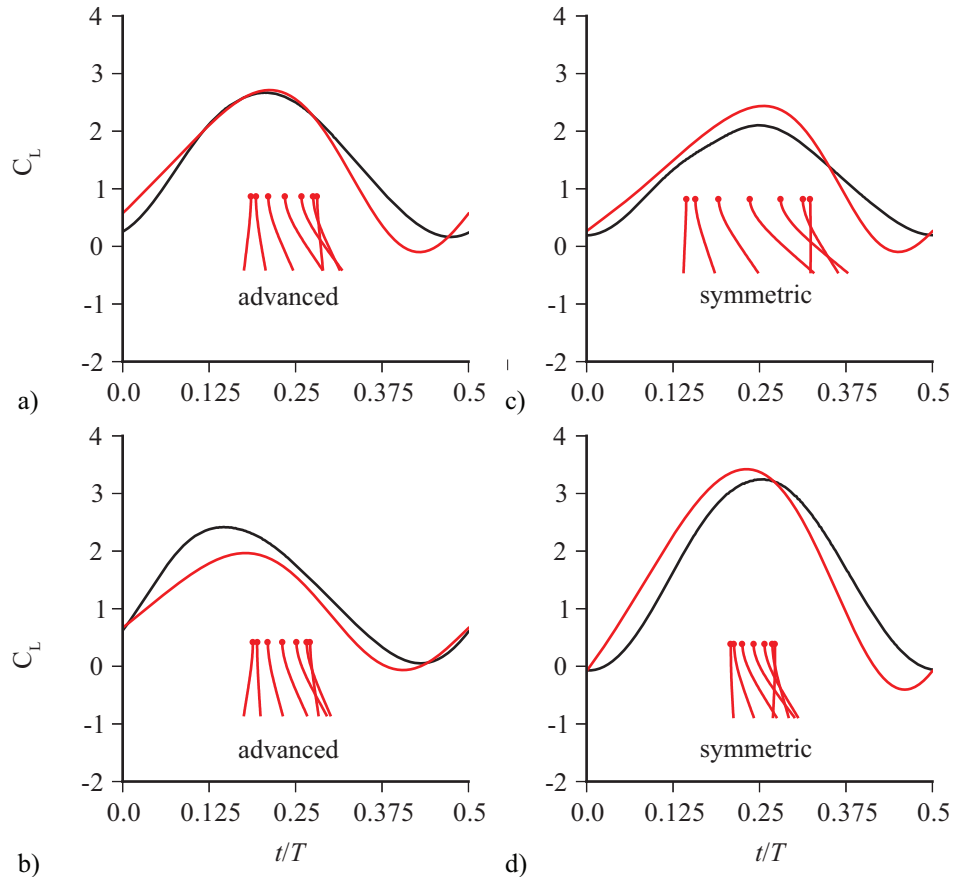

Figure 6. Representative time histories of the unsteady lift coefficient C_L for (a,b) two advanced rotation and (c,d) symmetric rotation cases. (−) Current quasi-steady model; (−) High fidelity model of Kang and Shyy[7].

Still, the resulting prediction of $C_L(t/T)$ captures the main trend with a good accuracy. A comparison of the time-averaged lift coefficient for all advanced and symmetric rotation modes are illustrated in Fig. 7a. While the quasi-steady model doesn't exactly match the lift predicted by the high fidelity model, the overall level of agreement is favorable. In particular, it is important to be able to predict the trend that as f/f_1 increases, higher lift is generated, reaching maximum when the resulting phase lag corresponds to a symmetric rotational mode $\varphi \approx 90°$, corresponding to $f/f_1 \approx 0.32$. The increasing trend of $\overline{C}_L$ as a function of f/f_1 is well captured by the current model as illustrated in Fig. 7a, which shows a comparison of the time-averaged lift coefficient for all advanced and symmetric rotation modes. Figure 7b shows the Mean-Squared Error (MSE) of $C_L(t/T)$, where

$$\text{MSE}(C_L) = \frac{1}{n}\sum_{i=1}^{n}\left(C_{L,pred} - C_{L,num}\right)^2, \tag{23}$$

where $n = 240$ is number of data points per half stroke, to quantify the difference between the predicted and numerical time histories of $C_L(t/T)$. The MSE increases with f/f_1, consistent with the departure from the several assumptions that we have used in this model. We modeled the fluid dynamic force coefficients with Eq. (19), which was obtained for a rigid wing without rotation. Also, the first-order harmonic representation of the passive pitch α_{FH} neglects the higher order transient response of the wing structure, which can contribute to the observed differences in the resulting lift[7].
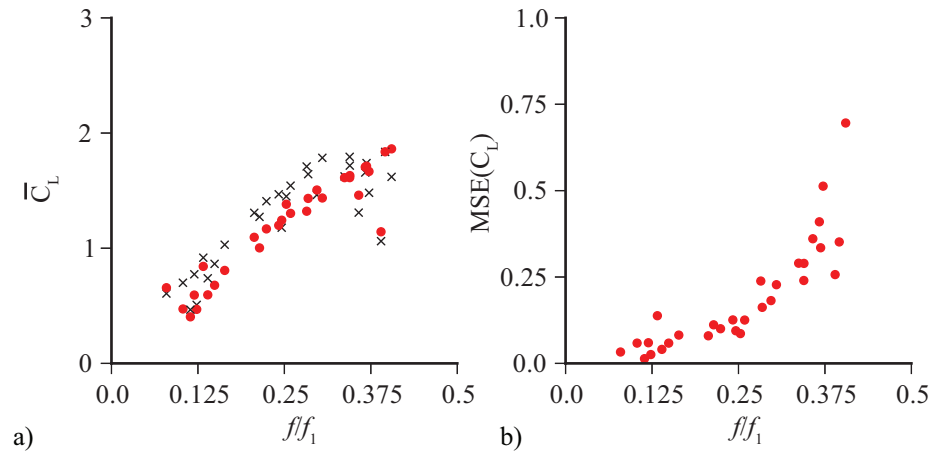
Figure 7. Integrated comparison of the unsteady lift generation. (a) Time-averaged lift coefficient of the unsteady lift coefficient $\bar{C}_L$: (●) Current quasi-steady model; (×) High fidelity model of Kang and Shyy[7] (b) Mean-squared error of the time histories of C_L.

IV. Concluding Remarks

This paper addresses modeling aspects of the unsteady lift and the corresponding response of the structural dynamics of a flapping, flexible wing at Re=100. We model the wing as a linear elastic flat plate and impose a sinusoidal plunge motion at the leading edge of the wing. Since the resulting wing motion is an outcome of the dynamic balance between the structural dynamics of the wing and the unsteady aerodynamics of the surrounding fluid, the wing kinematics is not known *a priori*. The chordwise deformations of the wing lead to displacements of the trailing edge relative to the leading edge of the wing, which can be considered as a passive pitch angle and affect the instantaneous angle of attack of the wing. In particular, the numerical solutions of a fully coupled aeroelastic framework indicate that relation between the passive pitch angle and the frequency ratio is complex.

Motivated by the scaling relationship between the γ-parameter and the time-averaged lift[3], we overcome this challenge by modeling the instantaneous passive pitch angle using the trailing edge deformations. The fluid dynamic force term is modeled by the Morison equation, in which the added mass force is proportional to the acceleration of the motion and the aerodynamic damping force depends on the square of the imposed translation. The predicted passive pitch angle at the end-of-the-stroke and the midstroke show a close agreement with the numerical solutions of a fully coupled aeroelastic framework. Based on these two angles, we construct the instantaneous passive pitch as a first-order harmonic by calculating the phase lag and the angular amplitude. The predicted amplitude and phase lag matched well with the numerical data, resulting in an excellent estimation of time evolution of the passive pitch.

The resulting unsteady lift on a flexible flapping wing can be obtained by applying the quasi-steady model for the imposed plunge motion if the modeled passive pitch can be modeled by the instantaneous wing velocities and accelerations, neglecting the influence from the history effects. For hovering motions, the nonlinear wing-wake interactions can have a substantial influence on the unsteady lift, although for a flexible wing these effects may be mitigated by the wing compliance.

The proposed model for unsteady lift takes in the *a priori* known scaling parameters, such as the reduced frequency and the frequency ratio, that depend on the wing thickness, wing density, and Young's modulus, as well as the imposed plunge amplitude as input. The use of dimensionless parameters enlarges the applicability of the proposed model for a wide range of parameters, regardless of the fluid media, wing structural properties, or imposed kinematics. We solve the beam equation for the wing deformations, coupled to the Morison equation accounting for both added mass and aerodynamic damping forces, to estimate the passive pitch angle at the end and mid-strokes. The instantaneous passive pitch angles are constructed based on these two angles and we use Dickinson's quasi-

American Institute of Aeronautics and Astronautics

steady model to estimate the lift on a flexible hovering wing. Despite all the simplifications involved in the model, the resulting time histories of lift agree favorably with the numerical data.

The fundamental limitations of such models are the lack of information of the key input parameters. The lift coefficient in the quasi-steady model and the aerodynamic damping coefficient in the Morison equations are empirically determined from various experiments. The major merit of this study is that based on the insight learned from the previously conducted high fidelity simulations, along with the empirical observations made in the literature, we have substantially enhanced the usefulness of the model by providing much improved predictive capability. These results are promising and may be highly relevant to understand the complex, but intriguing physics of flexible flapping wings. Also, such a model can become a valuable tool for an accurate model of the flight dynamics of a flapping wing Micro-Air Vehicles.

Acknowledgement

References

[1]Shyy, W., Aono, H., Kang, C., and Liu, H., *An Introduction to Flapping Wing Aerodynamics*, Cambridge University Press, New York, 2013.

[2]Fung, Y. C., *An Introduction to the Theory of Aeroelasticity*, Dover publications, inc., 2008.

[3]Kang, C., Aono, H., Cesnik, C. E. S., and Shyy, W., "Effects of Flexibility on the Aerodynamic Performance of Flapping Wings," *Journal of Fluid Mechanics*, Vol. 689, 2011, pp. 32–74.

[4]Kang, C.-K., and Shyy, W., "Modeling of Instantaneous Passive Pitch of Flexible Flapping Wings," *43rd AIAA Fluid Dynamics Conference and Exhibit, San Diego, California*, pp. AIAA–2013–2469.

[5]Trizila, P., Kang, C.-K., Aono, H., Shyy, W., and Visbal, M., "Low-Reynolds-Number Aerodynamics of a Flapping Rigid Flat Plate," *AIAA Journal*, Vol. 49, No. 4, 2011, pp. 806–823.

[6]Altshuler, D. L., Dickson, W. B., Vance, J. T., Roberts, S. P., and Dickinson, M. H., "Short-amplitude High-frequency Wing Strokes Determine the Aerodynamics of Honeybee Flight," *Proceedings of the National Academy of Sciences of the United States of America*, Vol. 102, No. 50, 2005, pp. 18213–18218.

[7]Kang, C., and Shyy, W., "Scaling Law and Enhancement of Lift Generation of an Insect-size Hovering Flexible Wing," *Journal of Royal Society Interface*, Vol. 10, No. 85, 2013.

[8]Shih, C. C., and Buchanan, H. J., "The Drag on Oscillating Flat Plates in Liquids at Low Reynolds Numbers," *Journal of Fluid Mechanics*, Vol. 48, No. 2, 1971, pp. 229–239.

[9]Sane, S., and Dickinson, M., "The Aerodynamic Effects of Wing Rotation and a Revised Quasi-steady Model of Flapping Flight," *Journal of Experimental Biology*, Vol. 205, No. 8, 2002, pp. 1087–1096.

[10]Wright, J. A., and Smith, R. W., "An Edge-based Method for the Incompressible Navier-Stokes Equations on Polygonal Meshes," *Journal of Computational Physics*, Vol. 169, 2001, pp. 24–43.

[11]Smith, R. W., and Wright, J. A., "An Implicit Edge-based ALE Method for the Incompressible Navier-Stokes Equations," *International Journal for Numerical Methods in Fluids*, Vol. 43, 2003, pp. 253–279.

[12]Luke, E. A., and George, T., "Loci: a Rule-based Framework for Parallel Multi-disciplinary Simulation Synthesis," *Journal of Functional Programming*, Vol. 15, No. 03, 2005, pp. 477–502.

[13]Balay, S., Brown, J., Buschelman, K., Gropp, W. D., Kaushik, D., Knepley, M. G., McInnes, L. C., Smith, B. F., and Zhang, H., "PETSc Web page," 2011.

[14]Balay, S., Brown, J., Buschelman, K., Eijkhout, V., Gropp, W. D., Kaushik, D., Knepley, M. G., McInnes, L. C., Smith, B. F., and Zhang, H., *PETSc Users Manual*, 2010.

[15]Falgout, R., and Yang, U., "hypre: A Library of High Performance Preconditioners," *Computational Science ICCS 2002*, edited by Sloot, P., Hoekstra, A., Tan, C., and Dongarra, J., Springer Berlin / Heidelberg, 2002, pp. 632–641.

[16]Thomas, P. D., and Lombard, C. K., "Geometric Conservation Law and its Application to Flow Computations on Moving Grids," *AIAA Journal*, Vol. 17, No. 10, 1979, pp. 1030–1037.

[17]Kamakoti, R., and Shyy, W., "Evaluation of Geometric Conservation Law using Pressure-based Fluid Solver and Moving Grid Technique," *International Journal of Heat and Fluid Flow*, Vol. 14, No. 7, 2004, pp. 851–865.

[18]De Boer, A., van der Schoot, M. S., and Bijl, H., "Mesh Deformation Based on Radial Basis Function Interpolation," *Computers & Structures*, Vol. 85, No. 11-14, 2007, pp. 784–795.

[19]Dickinson, M. H., Lehmann, F. O., and Sane, S. P., "Wing Rotation and the Aerodynamic Basis of Insect Flight," *Science*, Vol. 284, No. 5422, 1999, pp. 1954–1960.

American Institute of Aeronautics and Astronautics

[20]Bisplinghoff, R. L., Ashley, H., and Halfman, R. L., *Aeroelasticity*, Dover publications, inc., 1996.

[21]Ramananarivo, S., Godoy-Diana, R., and Thiria, B., "Rather than Resonance, Flapping Wing Flyers May Play on Aerodynamics to Improve Performance," *Proceedings of the National Academy of Sciences of the United States of America*, Vol. 108, No. 15, 2011, pp. 5964–5969.

[22]Saffman, P. G., *Vortex Dynamics*, Cambridge University Press, 1995.

[23]Thiria, B., and Godoy-Diana, R., "How wing compliance drives the efficiency of self-propelled flapping flyers," *Phys. Rev. E*, Vol. 82, No. 1, 2010, p. 15303.

[24]Dewey, P. a., Boschitsch, B. M., Moored, K. W., Stone, H. a., and Smits, A. J., "Scaling laws for the thrust production of flexible pitching panels," *Journal of Fluid Mechanics*, Vol. 732, 2013, pp. 29–46.

[25]Fry, S. N., Sayaman, R., and Dickinson, M. H., "The Aerodynamics of Hovering Flight in Drosophila.," *Journal of Experimental Biology*, Vol. 208, No. 12, 2005, pp. 2303–2318.

[26]Lehmann, F.-O., Gorb, S., Nasir, N., and Schützner, P., "Elastic Deformation and Energy Loss of Flapping Fly Wings," *Journal of Experimental Biology*, Vol. 214, No. 17, 2011, pp. 2949–61.

[27]Dickinson, M. H., Lehmann, F. O., and Götz, K. G., "The Active Control of Wing Rotation by Drosophila," *The Journal of Experimental Biology*, Vol. 182, 1993, pp. 173–89.

[28]Young, J., Walker, S. M., Bomphrey, R. J., Taylor, G. K., and Thomas, A. L. R., "Details of Insect Wing Design and Deformation Enhance Aerodynamic Function and Flight Efficiency," *Science*, Vol. 325, No. 5947, 2009, pp. 1549–52.

[29]Walker, S. M., Thomas, A. L. R., and Taylor, G. K., "Deformable Wing Kinematics in the Desert Locust: How and Why Do Camber, Twist and Topography Vary through the Stroke?," *Journal of the Royal Society, Interface*, Vol. 6, No. 38, 2009, pp. 735–747.

[30]Birch, J. M., and Dickinson, M. H., "The influence of wing-wake interactions on the productions of aerodynamic forces in flapping flight," *Journal of Experimental Biology*, Vol. 206, No. 13, 2003, pp. 2257–2272.